Research Article

Intelligent Optimization of Parameters for Tens of MA-Class Z-Pinch Accelerators

Siyuan Fan ⓘ,[1] **Hao Wei** ⓘ,[2] **Zhenzhou Gong**,[1] **Xu He**,[1] **Fengju Sun**,[2] and **Aici Qiu**[1]

[1]*State Key Laboratory of Electrical Insulation and Power Equipment, Xi'an Jiaotong University, Xi'an 710049, China*
[2]*State Key Laboratory of Intense Pulsed Radiation Simulation and Effect, Northwest Institute of Nuclear Technology, Xi'an 710049, China*

Correspondence should be addressed to Hao Wei; weihaoyy@sina.com

In order to minimize the initial energy storage of tens of MA-class Z-pinch accelerators, an intelligent optimization method was developed based on the transmission line code circuit model and PSOGSA algorithm. Using several input parameters, the four overall parameters of the Z-pinch accelerator could be fast determined, including the connection and parallel combination of LTD cavities, the outer radius of the stack-MITL system, and electrical length of monolithic radial transmission lines. The optimization method has been verified by comparing the results with the Z-300 and Z-800 conceptual designs. By means of this intelligent optimization, some factors that affect the initial energy storage on high-current Z-pinch accelerators have been investigated, such as the operating electrical fields, the diameter of the stack-MITL system, and the inner diameter of the LTD cavity. The suggestions for designing relatively low-cost, efficient LTD-based accelerators have been proposed.

1. Introduction

Significant progress in pulsed-power science and technology has been made in the past decades. A series of pulsed-power Z-pinch accelerators have been developed to support a wide variety of high-energy-density-physics experiments in the fields of radiation physics, plasma physics, equation of state, and inertial confinement fusion [1–4].

In recent years, many conceptual designs of Z-pinch accelerators using linear transformer drivers (LTD) [5, 6] as a prime power source have been proposed [7–11]. To clearly observe how the pulsed-power components behave and predict the output electrical parameters before experiments, circuit simulation and analysis are very important. A series of advanced circuit codes such as Screamer [12, 13], Bertha [14], and TLCODE [15] have been proposed, which were used to facilitate the conceptual design and better understanding of the complex systems.

For an LTD-based accelerator, the total number of LTD cavities is expected to be as small as possible in order to make the entire design more efficient and less expensive. In this

article, a self-consistent transmission line circuit model is developed for a high-current LTD-based pulsed-power accelerator. A hybrid population-based algorithm PSOGSA [16] is implemented to optimize some of the overall architecture parameters, including the connection and parallel combination of LTD cavities, the outer radius of the stack-MITL system, and the electrical length of the monolithic radial transmission lines.

The remainder of this article is organized as follows. Section 2 gives a detailed description of the circuit model and the full calculation process. In Section 3, the optimization method is validated by comparing the results with the conceptual design of Z-300 and Z-800. In Section 4, several factors that affect the initial energy storage are investigated. Section 5 gives several suggestions for the future design of the pulsed-power accelerators. Conclusions are given in Section 6.

2. Circuit Model and Optimization Method

2.1. Circuit Model of LTD-Based Z-Pinch Accelerators.
Figure 1 shows a general schematic of an LTD-based accelerator. The structure in this figure is a four-level
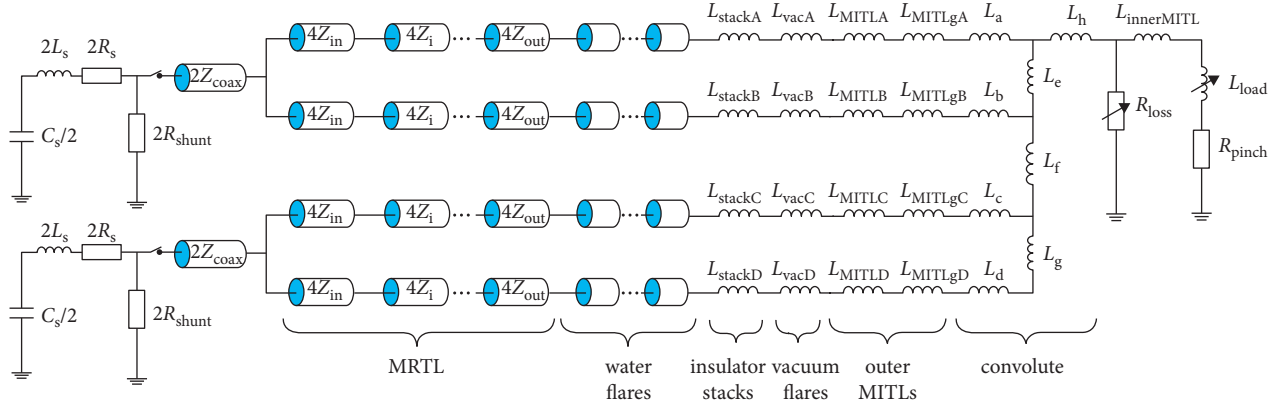
FIGURE 1: General schematic of the circuit model. The structure in this figure is a four-level transmission line system, other options are available in the model like two or six levels. The center vacuum section from A–D level is simulated by lumped inductances, L_{MITL} and L_{MITLg} denote the inductances of the constant impedance section of MITL and constant gap section of MITL, respectively.

transmission line system, other options are available in the model like two or six levels. The electrical pulse is primarily generated by the multi-LTD modules, which are piled up in one to three levels, each LTD module drives an internal water-insulated coaxial transmission line. The impedance profile of the internal transmission line should be matched to the LTD module to maximize the peak forward-going power. In Figure 1, the multi-LTD modules are piled up in two levels and each level is considered identical.

The equivalent resistance R_s, inductance L_s, and capacitance C_s of the whole prime power source are determined by (1)–(3), where n_b is the number of LTD bricks within a single LTD cavity, n_c is the number of LTD cavities connected in series within each LTD module, and n_m is the number of LTD modules in parallel. And R_b, L_b, and C_b are the equivalent resistance, inductance, and capacitance of a single LTD brick, respectively. The shunt resistances (4) are also included in the model to account for the ferromagnetic core losses, it is assumed as a constant resistance R_c (~45 Ω) within each cavity, whose value is much greater than the impedance of a single LTD cavity.

$$R_s = \frac{n_c}{n_b n_m} R_b, \tag{1}$$

$$L_s = \frac{n_c}{n_b n_m} L_b, \tag{2}$$

$$C_s = \frac{n_b n_m}{n_c} C_b, \tag{3}$$

$$R_{shunt} = \frac{n_c}{n_m} R_c. \tag{4}$$

At the output of the LTD module, each LTD module drives a water-insulated coaxial transmission line, and the coaxial line could be a uniform line or an impedance transformer. Then, these coaxial transmission lines merge into monolithic radial transmission lines (MRTLs). The monolithic radial transmission lines are impedance transformers, which drive the insulator stacks and magnetically

insulated transmission lines (MITLs), and ultimately, the physics load at the center of the accelerator.

The input impedance of the coaxial water transmission line is equivalent to the output impedance of the whole LTD system, which is expressed as [9].

$$Z_{coax,input} = Z_{LTD} = 1.1\sqrt{\frac{Ls}{Cs}} + 0.8R_s. \tag{5}$$

It is assumed here that each level of MRTLs is identical. The resistivity ρ_w of the water used to insulate the MRTLs is 3×10^4 Ω·m. And the influence of electrode resistance loss is neglected as it is very slight. The output impedance Z_{out} of the MRTLs is to be calculated iteratively in the model, and is constrained by several limitations:

(1) It is usually required that Z_{out} should not be smaller than Z_{in}.

(2) The electric field is the highest near the output of the impedance transformer. The minimum AK gap at the outlet of the MRTL should be satisfied with the water insulation criterion [17]:

$$E_{max}\tau_{eff}^{0.33} = \frac{U_{out}}{h_{out}}\tau_{eff}^{0.33} \leq 0.113, \tag{6}$$

where E_{max} is the average peak electric field at the output of the MRTL in MV/cm, τ_{eff} is the temporal width of the voltage pulse at 63% of peak value, which is in μs, U_{out} and h_{out} are the MRTL peak output voltage and the AK gap at the output, respectively.

(3) The plastic-vacuum interface has the lowest limit on the electric field in the pulsed-power system. Therefore, the AK gap at the output of the MRTL should not exceed the height of the insulator stack.

Since the MRTL is usually a nonuniform transmission line, it can be considered as a cascaded multiple segment line, and each segment line has the same electric length but a different impedance. There is a short water-insulated transmission line (water flare) between the MRTL outlet and

TABLE 1: List of parameters.

LTD source parameters	R_b (Ω)	L_b (nH)	C_b (nF)	n_b	V_b (kV)	D_{cav} (m)	D_{inner} (m)	l_{cav} (m)
Transmission line parameters	level n	h_p (cm)	h_r (cm)	E_{ave} (kV/cm)	Z_{MITLs} (Ω)	θ_1 (°)		
Load parameters	r_0 (cm)	h_{load} (cm)	$L_{load}(0)$ (nH)	m_{load} (mg)	CR			

the insulator stack at each level, which is also simulated by several transmission line elements.

The breakdown limit of the vacuum interface of the insulator stack should be considered in the model. The number and height of insulators and grading rings are conservative in the design to prevent insulator flashover. In the numerical calculations discussed later, with the initial guess of stack voltage and the given heights of the insulator rings and grading rings, the number of them will be determined iteratively to achieve relatively low inductance at this portion, which also determines the height of the insulator stack.

In order to increase the calculation efficiency, the insulator stacks, the vacuum flares, the magnetically insulated transmission lines, the post-hole convolute, and the inner MITL are simulated as several lumped inductances, as demonstrated in Figure 1. An inductance calculation method is embedded in the circuit model, the inductance of each portion can be obtained through iterative calculations with initial parameters generated by upstream circuit elements. This calculation method has been examined and validated by comparing the results from Z, PTS, and Z-300/Z-800 [18]. The physics load considered in our simulation is a tungsten wire array for Z-pinch, which is simulated as a time-dependent inductance and a constant pinch resistance. The plasma implosion of the Z-pinch load is simulated by the 0-D model, and the pinch resistance is assumed constant as 5 mΩ/cm [19].

A shunt resistor R_{loss} is set between the post-hole convolute and the inner MITL to model the electron flow current lost to the anode of the convolute and inner MITL [20]. R_{loss} is controlled by a "Z-flow" element, whose value is determined by the vacuum impedances of outer MITLs and the gap closure effects are included.

$$R_{loss} = Z_{flow}\sqrt{\frac{(I_a + I_c)}{(I_a - I_c)}}. \tag{7}$$

2.2. Optimization Method. PSOGSA is a hybrid optimization algorithm proposed by Mirjalili and Hashim [16], and it balances the advantages of PSO (particle swarm optimization) [21, 22] and GSA (gravitational search algorithm) [23]. In our case, it is expected that with a given peak load current and assumed load implosion time, the algorithm could search for a minimum number of total LTD cavities, which implies how much energy needs to be stored primarily at least by the accelerator's capacitors to meet the requirements of the experiment, which could make the entire design less expensive and more efficient. Therefore, the fitness function in the optimization is

TABLE 2: Parameters that need to be determined from optimization method.

Parameters	Min	Max
n_c	6	(10)
n_m	6	180
T_{line} (ns)	(11)	500
$r_{waterflare}$ (m)	1.3	3

$$\text{fitness} = n_c n_m. \tag{8}$$

The basic parameters of the circuit model consist of three parts: LTD prime power source parameters, transmission line system parameters, which include water transmission lines and magnetically insulated transmission lines, and load parameters, as listed in Table 1. These values need to be settled prior to the start of the numerical simulation. Note D_{cav}, D_{inner}, and l_{cav} are the outer diameter and the inner diameter (anode diameter) and length of a single LTD cavity, respectively, Vb is the LTD charge voltage across a single brick, n is the level of the transmission line system, h_p and h_r are the height of a single insulator ring and a grading ring, E_{ave} is the maximum mean electric field allowed at the insulator stack, Z_{MITLs} are the vacuum impedances of outer MITLs, and θ_1 is the angle of the upper cathode of MITL. For load parameters, CR denotes the convergence ratio of the imploding load. With the desired peak load current I_p and load implosion time τ_i, the required total initial mass of the load can be estimated by the scaling relation [24, 25]:

$$m_{load} \propto \frac{I_p^2 \tau_i^2 h_{load}}{r_0^2}, \tag{9}$$

where h_{load} and r_0 are the height and initial radius of the Z-pinch load.

There are four major parameters that need to be determined in the circuit simulation with PSOGSA: the number of LTD cavities connected in series n_c, the number of LTD modules in parallel n_m, the electrical length of water-insulated monolithic radial transmission lines T_{line}, and the radius of the stack-MITL system $r_{waterflare}$ as listed in Table 2. Their values should be limited to a reasonable range. The upper limit of n_c is totally constrained by the LTD cavity parameters mentioned above and the water insulation criterion:

$$d = 0.5\left(D_{inner} - D_{cathode}\right) \times 100, \tag{10a}$$

$$n_c Z_{cav} = \frac{60}{\sqrt{\varepsilon_r}}\ln\left(\frac{D_{inner}}{D_{cathode}}\right), \tag{10b}$$

$$\frac{n_c U_p}{d}\tau_{LTD}^{0.33} \leq 0.113, \tag{10c}$$

where U_{p} is the peak output voltage (in MV) of a single LTD cavity when connected to a matched load, d is the AK gap in cm, Z_{cav} is the impedance of a single LTD cavity, D_{cathode} is the cathode diameter of the LTD module at the outlet, and τ_{LTD} is the effective pulse width (in μs) of the voltage pulse at 63% of peak when the single LTD cavity is terminated to a matched load.

The lower limit of T_{line} is determined by the number of LTD modules in parallel per level, the electrical length of coaxial transmission line Tcoax, and the outer diameter of the LTD cavity and the stack-MITL system (Note level n= 2, 4, 6):

$$T_{\mathrm{line}} \geq \frac{(n_m D_{\mathrm{cav}}/\pi n) - r_{\mathrm{waterflare}}}{c} \sqrt{\varepsilon_r} - T_{\mathrm{coax}}. \quad (11)$$

The full calculation flow chart is illustrated in Figure 2. At the beginning of the calculation, three parts of the basic parameters and the desired peak load current, and load implosion time are inserted into the algorithm, then PSOGSA starts to initiate many sets of values of n_{c}, n_{m}, T_{line}, and $r_{\mathrm{waterflare}}$ within the reasonable range, which are considered as " particle positions" in PSOGSA. With previous parameters, two initial voltage values $U(0)$ stack, $U(0)$ out and an initial estimated effective pulse width $\tau(0)$ eff for the subsequent iterative calculations are generated. $U(0)$ stack includes the initial guesses of peak voltage at the stack at each level. $U(0)$ out is the initial guess of peak voltage at the MRTL outlet (input of the water flare) at the lowest level. $\tau(0)$ eff is the effective pulse width of the voltage pulse at 63% of the peak at the MRTL outlet. $U(0)$ stack, $U(0)$ out, and $\tau(0)$ eff can be estimated by the following scaling relations:

$$U_{\mathrm{stack}}^{(0)} \propto \left(\frac{I_p}{\tau_i}\right)^{\frac{5}{3}},$$

$$U_{\mathrm{out}}^{(0)} \propto n_c V_b, \quad (12)$$

$$\tau_{\mathrm{eff}}^{(0)} \propto \sqrt{L_b C_b}.$$

$U(0)$ out and $\tau(0)$ eff determine the minimum AK gap at the MRTL outlet with (6), as the peak voltage at the MRTL outlet at the lowest level is the largest among all levels, this AK gap in other levels will also meet the requirement given by (6), then MRTL output impedance Z_{out} is obtained with this AK gap and $r_{\mathrm{waterflare}}$ by:

$$Z_{\mathrm{out}} = \frac{60 h_{\mathrm{out}}}{n \times \sqrt{\varepsilon_r} \times r_{\mathrm{waterflare}}}. \quad (13)$$

The value of $U(0)$ stack, $r_{\mathrm{waterflare}}$, and E_{ave} are inserted into the inductance calculation method mentioned above, the number of insulators and grading rings are determined by $U(0)$ stack, E_{ave}, and h_{p}. The height of the insulator stack for each level is therefore obtained. Then, the geometry and circuit elements for water flares can be determined to connect the MRTL and the stack. Then with Z_{MITLs}, θ_1, $r_{\mathrm{waterflare}}$, the height of the stacks, preset vacuum flare radial distance, minimum AK gaps allowed in MITLs, and other

basic settled parameters, the geometry of each MITL level and the inductance of each portion in the vacuum stack-MITL system are distinguished and calculated [18].

At this point, all circuit elements needed in the model are completed. The circuit model is run for the first time and generates three new values as $U(1)$ stack, $U(1)$ out, and $\tau(1)$ eff. The loop continues until the differences between these values obtained from two adjacent iteration loops are within the limit of error (<0.05 MV for voltages, <5 ns for pulse width), which means these three values converge. After all of the candidate positions are calculated in the model, the circuit simulation is finished in the first big iteration of PSOGSA. The current best position and fitness are found. The PSOGSA algorithm will continue to calculate the particle masses, gravitational forces, particle accelerations, and update sets of velocities and positions to search for better solutions until the fitness value remains unchanged.

3. Validation of Optimization Method

To compare the result from this model with conceptual designs outlined in [10], the basic parameters are set exactly the same as Z-300 in the circuit model, it is noted that there is no coaxial line at the output of LTD modules in Z-300 design, the vacuum impedances of six MITLs are all $5\,\Omega$, the maximum mean electric field E_{ave} allowed at the stack is 200 kV/cm, the outer radius of the stack-MITL system $r_{\mathrm{waterflare}}$ is 2.59 m, and the electrical length of MRTL is 230 ns, only parameters n_{c} and n_{m} remain unknown. The upper limit of n_{c} for Z-300 is 36 according to (10a)–(10c) in the simulation for the 0.8 m LTD cavity inner diameter under $\pm 100\,\mathrm{kV}$ charge voltage. The optimization simulation gave close results to Z-300 shot conducted with a MagLIF load (Desired peak load current is 48 MA, load length = 1 cm, initial radius = 0.5 cm, load mass = 444 mg). The simulation result indicated 2856 LTD cavities in total, as shown in Table 3, together with the simulation result for Z-800. The total inductance L_{center} of the central vacuum section for Z-300 is 20.41 nH when the load is imploded to its final radius, which is almost the same as the 20.2 nH value given by [10]. Note η denotes the accelerator efficiency, which can be calculated as follows [10]:

$$\eta = \frac{K_f}{E_s} + \frac{0.5\left(L_{\mathrm{inner}} + L_{\mathrm{load},f}\right)I_f^2}{E_s}, \quad (14)$$

where K_f is the final kinetic energy of the load, L_{inner} is the inner MITL inductance; $L_{\mathrm{load},f}$ and I_f are the load inductance and load current at the moment of stagnation, respectively; and E_{s} is the initial energy stored in the LTD system.

4. Influences to the Initial Energy Storage

4.1. Influence of Maximum Allowed Mean Electric Field. In this section, the influence of the maximum mean electric field E_{ave} allowed at the insulator stack to the required minimum initial energy storage is investigated. The equivalent resistance R_{b}, inductance L_{b}, and capacitance C_{b} of a single LTD brick are $0.3\,\Omega$, 200 nH, and 50 nF, respectively. Each LTD cavity is a right-circular annulus with an outer
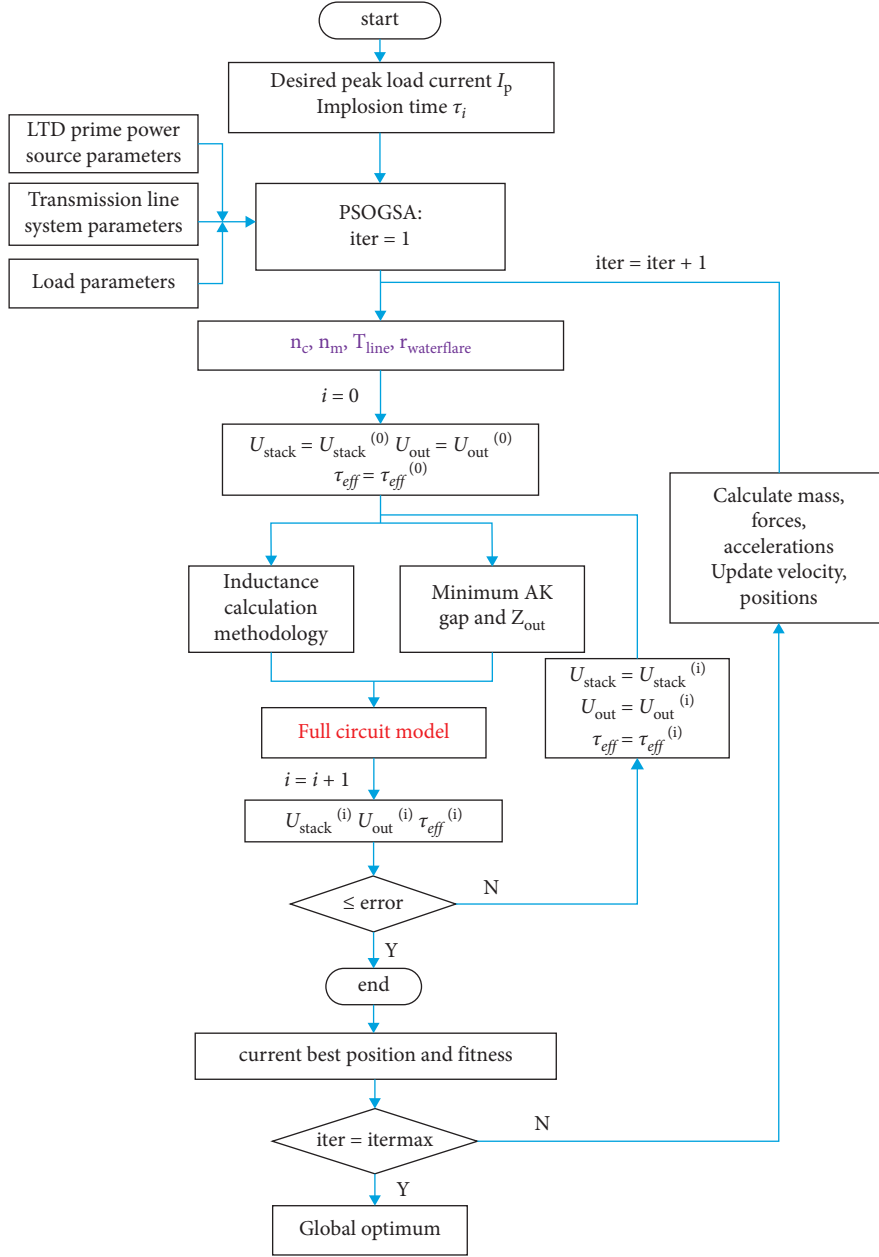
FIGURE 2: Full calculation flow chart.

diameter of 2.3 m, an inner diameter of 0.91 m, and a length of 0.22 m, which contains 23 LTD bricks. At the output of each LTD module, a 90 ns uniform coaxial water-insulated transmission line is connected to provide 180 ns transit-time isolation between adjacent LTD modules. The height of insulator rings and grading rings are 5 and 0.8 cm, respectively. A four-level transmission line system is adopted, and the vacuum impedances of four MITLs are 2, 2, 3, and 3 Ω, and $\theta_1 = 15°$. The Z-pinch load is a wire array with an initial radius of 2 cm and a length of 2 cm, the initial inductance of the load is 1.1 nH, and the convergence ratio is assumed as 10:1. The target peak load current is 30 MA and the implosion time is 157 ns, hence the total initial load mass is chosen as ~20.7 mg with (9). Figure 3 shows the minimum LTD cavity number

versus the maximum allowed mean electric field E_{ave} under different charge voltages. It is seen that the total number of cavities decreases with the increase in E_{ave}, and it is obvious that the number of cavities can be greatly reduced with larger charge voltages. As E_{ave} increases from 100 to 200 kV/cm, the number of insulators needed decreases with the increase of E_{ave}, the total initial inductance L_{center} of the stack-MITL system is consequently reduced from ~14.4 to ~11.6 nH, the LTD cavity number is reduced by ~14%. Note L_{center} also includes the inductance of the water flares. In these sets of simulations, the MRTL electrical length and radius of the stack-MITL system are free values within reasonable ranges as illustrated in Table 2. Their influences are further studied in Section 4.2 and Section 4.3.

TABLE 3: Comparison of simulation results with Z-300 and Z-800. The symbol "*" denotes the simulation result from this article.

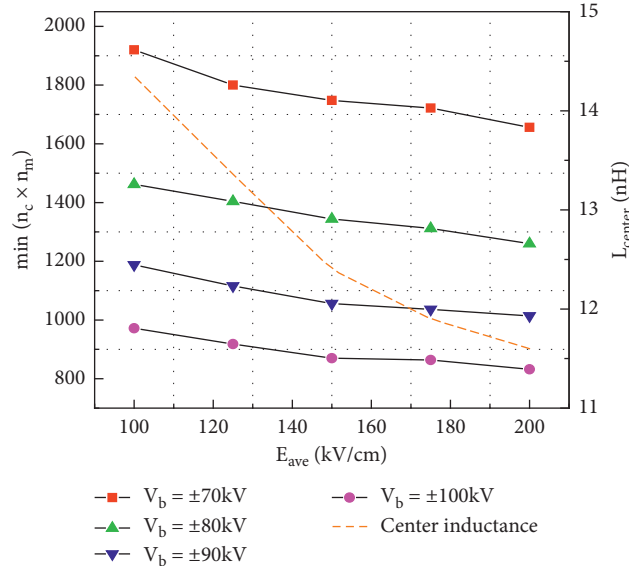| Facility	n_c	n_m	min ($n_c \times n_m$)	Z_{in} (Ω)	Z_{out} (Ω)	L_{center} (nH)	I_{max} (MA)	η (%)	Accelerator diameter (m)
Z-300*	34	84	2856	0.049	0.173	20.41	48.1	24.4	36
Z-300 [10]	33	90	2970	0.044	0.165	20.2	48	24	35
Z-800*	69	72	4968	0.078	0.302	23.79	65.1	17.6	56
Z-800 [10]	60	90	5400	0.054	0.290	23.59	65	17	52

FIGURE 3: Minimum LTD cavity number versus the maximum allowed mean electric field E_{ave} under different charge voltages.

TABLE 4: Minimum LTD cavity number varies with different MRTL electrical lengths.

T_{line} (ns)	min ($n_c \times n_m$)	n_c	n_m	Z_{in} (Ω)	Z_{out} (Ω)	L_{center} (nH)	I_{max} (MA)	η (%)
112	1296	27	48	0.060	0.214	14.70	30.0	20.0
200	1102	29	38	0.081	0.217	14.72	30.1	23.7
300	1064	28	38	0.078	0.217	14.72	30.0	24.4
350	1044	29	36	0.085	0.217	14.72	30.0	24.8
400	1044	29	36	0.085	0.217	14.72	30.0	24.9

TABLE 5: Minimum LTD cavity number varies with different radius of the stack-MITL system.

$r_{waterflare}$ (m)	Min ($n_c \times n_m$)	n_c	n_m	Z_{in} (Ω)	Z_{out} (Ω)	L_{center} (nH)	U_{stack} (MV)	I_{max} (MA)	η (%)
1.7	1392	29	48	0.064	0.282	16.39	5.72	30.2	19.0
1.9	1160	29	40	0.077	0.231	14.94	5.19	30.1	22.6
2.1	1102	29	38	0.081	0.206	14.46	5.07	30.2	23.7
2.3	1044	29	36	0.085	0.185	14.33	4.94	30.1	25.1
2.5	1008	28	36	0.083	0.165	14.03	4.79	30.1	25.9
2.7	986	29	34	0.090	0.153	14.04	4.77	30.1	26.4
2.9	986	29	34	0.090	0.144	14.11	4.77	30.2	26.7
3.1	986	29	34	0.090	0.136	14.23	4.78	30.1	26.5

4.2. Influence of Electric Length of MRTL. In this section, the charge voltage is fixed to ±100 kV, then the upper limit of LTD cavities connected in series should not exceed 29 according to (10a)–(10c). The maximum mean electric field E_{ave} allowed at the insulator stack is set to 100 kV/cm, other parameters remain the same as in Section 4.1. Table 4 shows the influence of MRTL electrical length when $r_{waterflare}$ is

fixed to 2 m. The minimum number of LTD cavities decreases with the increases in T_{line} because the power transport efficiency of MRTL increases with the increase of T_{line}. But the electrical length should not be lengthened too much, because the influence of water dielectric losses will be more remarkable when T_{line} is getting longer, and the improvement to power transport efficiency will be
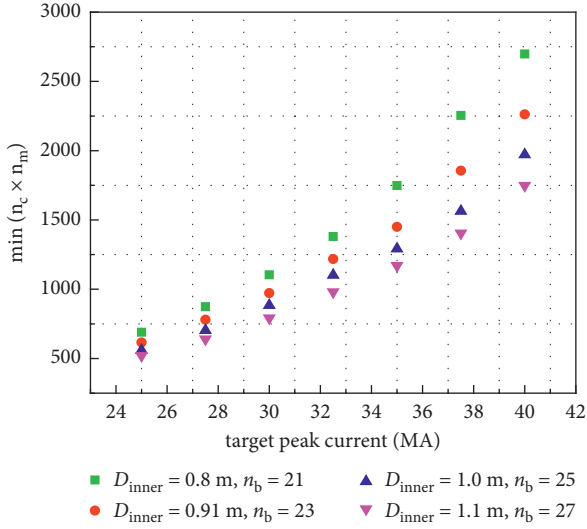
FIGURE 4: Minimum LTD cavity number versus peak load currents with different inner diameters of the LTD cavity.

inconspicuous. The longer MRTL also requires a larger diameter of the entire accelerator and increases the cost.

4.3. Influence of the Outer Radius of Stack-MITL System. The individual influence of the outer radius of the stack-MITL system is investigated when the electrical length of MRTL is fixed to 180 ns, as shown in Table 5 (Note Eave is still 100 kV/cm). It is seen that the minimum number of cavities decreases dramatically first in the given range of $r_{\text{waterflare}}$ and then becomes insensitive to $r_{\text{waterflare}}$. Because the total initial center inductance L_{center} decreases at the beginning as the stack inductance is reduced with the increase in $r_{\text{waterflare}}$, and the MRTL output impedance keeps decreasing with the increase in $r_{\text{waterflare}}$, which improves the impedance matching in the MRTL (the ratio of $Z_{\text{out}}/Z_{\text{in}}$ decreases) and increases the power transport efficiency. But when $r_{\text{waterflare}}$ is large enough, the center inductance will increase slowly with the same variation trend of peak stack voltage (Table 5 shows the peak stack voltage at the lowest level), because the increase of inductance in outer MITLs becomes more significant, which limits the performance of the whole system.

4.4. Influence of the Inner Diameter of the LTD Cavity. In this section, the influence of the inner diameter (anode diameter) of the LTD cavity is investigated. The number of LTD bricks per cavity (n_b) is different with different cavity inner diameters. T_{line} and $r_{\text{waterflare}}$ are free values within reasonable ranges as illustrated by Table 2. The charge voltage is fixed to ±100 kV, as the D_{inner} increases from 0.8 to 1.1 m, the upper limit of n_c increases from 23 to 40 according to (10a)–(10c), which makes it possible for more cavities connected in series within each module. The minimum number of LTD cavities versus target peak load currents with different D_{inner} is shown in Figure 4. The total number of cavities decreases with the increase in D_{inner}, as more LTD

cavities can be connected in series within each module and fewer modules are arranged in parallel, the input impedance of MRTL increases, which also improves the impedance matching in the MRTL. And with a higher target peak load current, the reduction of cavity number is more remarkable with the increase in D_{inner}. For example, the cavity number is decreased by 950 (total LTD bricks are reduced by 9462) if the inner diameter of the cavity increases from 0.8 to 1.1 m for a 40 MA target peak current, as detailed in Table 6.

The methods mentioned above can be used to optimize the *Z-300/Z-800* design. First, when the electrical length of MRTL and the radius of the stack-MITL system are free values, simulation results will be better than in Table 3, as indicated by the second and fourth row in Table 7. If the inner diameter increases from 0.8 to 0.9 m for *Z-300* (number of bricks per cavity remains unchanged), the upper limit of n_c becomes 51, the cavity number is further reduced to 2565, as indicated by the third row. If the inner diameter increases from 1.3 to 1.4 m for *Z-800*, the upper limit of n_c becomes 84, the cavity number is reduced to 4686, as indicated by the fifth row.

5. Suggestions for Future Design

Figure 5 shows the minimum number of cavities versus target peak load currents with ±100 kV charge voltage and the same prime power source parameters given in Section 4, and the maximum mean electric field allowed at the stack is 100 kV/cm. The minimum electric length of MRTL is set as 150 ns to make transit-time isolation between the stack and the LTD modules (Note there are no coaxial lines at the output of LTD modules in this section). When the number of modules in parallel is large enough that 150 ns long MRTL is not sufficient, the electric length of MRTL is assumed as the lower limit with (11) to make the scale of the accelerator as compact as possible. The vacuum impedances of MITLs are assumed as 2 and 4.5 Ω for each level in two-level transmission line system and six-level transmission line system, respectively. The trend of the relation in Figure 5 is close to a power-law that the initial energy storage is proportional to $I_p^{8/3}\tau_i^{-2/3}\eta_t^{-1}$ [9], where η_t is the power transport efficiency of the impedance transformers, τ_i is fixed as ~157 ns. The choice of the level of transmission line system when the target peak load current is in the range of 10–15 MA and 35–50 MA is a dilemma. For example, when the target peak current is 15 MA, using a two-level transmission line system and a four-level transmission line system requires 234 and 196 cavities, respectively. Although a four-level transmission line system requires fewer cavities, the electron flow loss is more significant than a two-level system. Because the flow impedance of a two-level MITL system is larger than a four-level system, as the vacuum impedance of a two-level MITL is 1 Ω (against 0.6 Ω in a four-level MITL system). But the center inductance of a two-level system is much higher than a four-level and it augments dramatically with the increase of target peak load current, as indicated in Figure 6. Therefore, when the target peak load current is large, a two-level system is no longer appropriate.

TABLE 6: Simulation results with different inner diameters of the LTD cavity for a 40 MA target peak load current.

D_{inner} (m)	n_b	max (n_c)	n_c	n_m	min $(n_b \times n_c \times n_m)$	Z_{in} (Ω)	Z_{out} (Ω)	$r_{waterflare}$ (m)	T_{line} (ns)	L_{center} (nH)	U_{stack} (MV)	I_{max} (MA)	η (%)
0.8	21	23	19	142	56658	0.016	0.216	3.0	595	16.91	7.77	40.0	18.8
0.91	23	29	29	78	52026	0.039	0.212	3.0	385	16.47	7.51	40.1	20.5
1.0	25	34	34	58	49300	0.057	0.214	2.96	311	16.48	7.44	40.0	21.8
1.1	27	40	38	46	47196	0.075	0.214	2.98	353	16.48	7.41	40.0	22.7

TABLE 7: Simulation results for Z-300 and Z-800 conceptual designs with more free variables and a larger inner diameter of cavity.

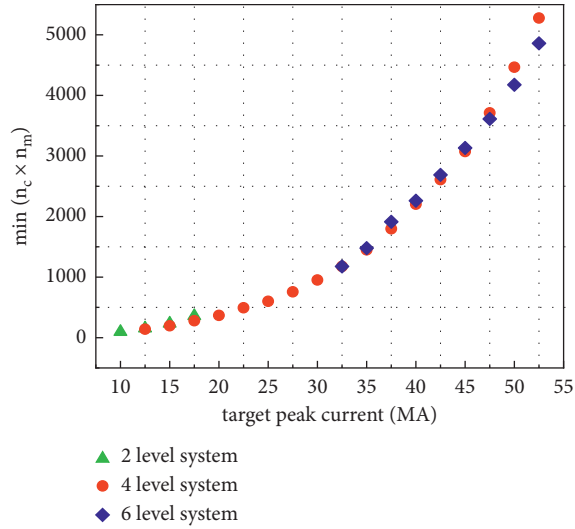| Facility	max (n_c)	n_c	n_m	min $(n_c \times n_m)$	Z_{in} (Ω)	Z_{out} (Ω)	$r_{waterflare}$ (m)	T_{line} (ns)	L_{center} (nH)	I_{max} (MA)	η (%)	Accelerator diameter (m)
Z-300 ($D_{inner} = 0.8$ m)	36	36	75	2700	0.059	0.176	2.52	316	20.33	48.2	25.8	42
Z-300 ($D_{inner} = 0.9$ m)	51	45	57	2565	0.096	0.181	2.45	297	20.25	48.1	27.1	45
Z-800 ($D_{inner} = 1.3$ m)	70	68	72	4896	0.077	0.284	2.99	323	23.87	65.1	17.9	58
Z-800 ($D_{inner} = 1.4$ m)	84	71	66	4686	0.087	0.286	2.93	449	23.88	65.1	18.5	67

FIGURE 5: The minimum number of cavities versus target peak load current with different transmission line systems.

FIGURE 6: The total initial inductance of the center section versus target peak load current with different transmission line systems.

In most cases, a four-level system requires almost the same cavity number as a six-level system does, as the center inductances of them are very close. But when I_p exceeds 45 MA, it is seen that the growth trend in cavities and central inductance of a four-level system exceeds the six-level system. As more LTD modules are arranged in parallel with the increasing target peak current, piling up the LTD modules in two layers when the four-level system is used usually requires a larger diameter of the accelerator than the six-level system (LTD modules piled up in three layers), as indicated by Figure 7. For example, using a four-level system requires 106 modules in parallel (3074 cavities in total) when the target peak load current is 45 MA, the outer diameter of
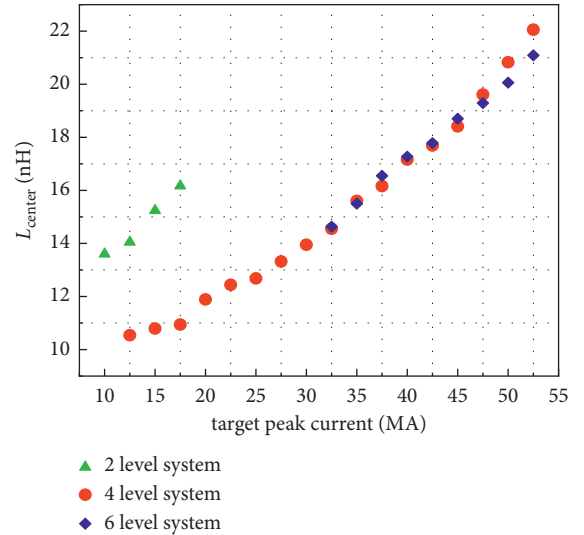
the whole machine is 52 m, in which case the electric length of MRTLs should be at least 488 ns. In contrast, using a six-level system requires 108 modules in parallel (3132 cavities in total), although it demands a little bit more cavities in total, the outer diameter of the whole machine is reduced to 39 m. Figure 8 demonstrates that the MRTL output impedance for a six-level system is much smaller than a four-level system, which usually makes it closer to the optimum impedance of maximizing the energy coupling efficiency to the stack-MITL system, which also indicates the better impedance match of MRTL in a six-level system. Moreover, when the voltage in the vacuum section is high enough, it is better to use relatively high vacuum impedance MITLs with
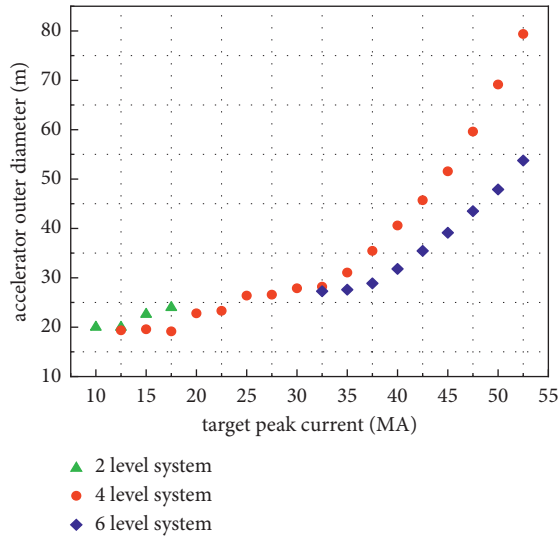
FIGURE 7: The outer diameter of the accelerator versus target peak load current with different transmission line systems.
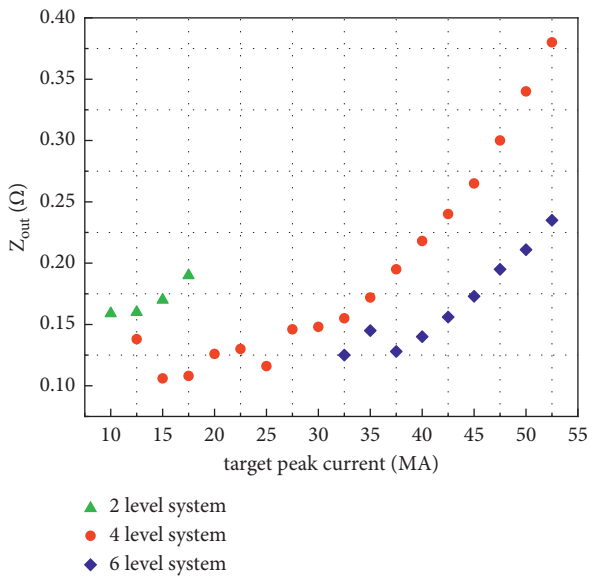

FIGURE 8: The output impedance of MRTL versus target peak load current with different transmission line systems.

more levels in consideration of safer operations for MITLs. Therefore, the consideration of center section inductance, the cost of MITLs, total current loss in MITLs, energy transport efficiency, accelerator diameter, electric length of MRTL, and output impedance of MRTL should be comprehensive when designing a large driver.

6. Conclusions

An iterative, self-consistent circuit model for high current Z-pinch accelerator is established in this article, the PSOGSA hybrid algorithm is implemented to help optimize the LTD prime power source, monolithic radial transmission lines, and stack-MITL parameters of the accelerator. Several factors that

might influence the minimum initial energy storage are investigated. Developing insulator stacks with higher flashover strength, adjusting the electric length of MRTL and the radius of the stack-MITL system, using higher impedance LTD modules can be used to optimize the performance of Z-300 and Z-800 conceptual designs and other similar high current Z-pinch accelerators. The regulations obtained from simulations would help us better understand the pulsed-power systems and provide predictions before the experiments.

Data Availability

The data that support the findings of this study are available from the corresponding author upon reasonable request.

Conflicts of Interest

The authors declare that they have no conflicts of interest.

Acknowledgments

References

[1] S. A. Slutz, M. C. Herrmann, R. A. Vesey et al., "Pulsed-power-driven cylindrical liner implosions of laser preheated fuel magnetized with an axial field," *Physics of Plasmas*, vol. 17, no. 5, Article ID 056303, 2010.

[2] B. Jones, J. P. Apruzese, A. J. Harvey-Thompson et al., "The effect of gradients at stagnation on K-shell x-ray line emission in high-current Ar gas-puff implosions," *Physics of Plasmas*, vol. 22, no. 2, Article ID 020706, 2015.

[3] J. E. Bailey, G. A. Chandler, D. Cohen et al., "Radiation science using Z-pinch x rays," *Physics of Plasmas*, vol. 9, no. 5, pp. 2186–2194, 2002.

[4] M. R. Martin, R. W. Lemke, R. D. McBride et al., "Solid liner implosions on Z for producing multi-megabar, shockless compressions," *Physics of Plasmas*, vol. 19, no. 5, Article ID 56310, 2012.

[5] B. M. Kovalchuk, V. A. Vizir, A. A. Kim et al., "Fast primary storage device utilizing a linear pulse transformer," *Russian Physics Journal*, vol. 40, no. 12, pp. 1142–1153, 1997.

[6] A. N. Bastrikov, V. A. Vizir, S. N. Volkov, V. G. Durakov, A. M. Efremov, V. B. Zorin, A. A. Kim, B. M. Kovalchuk, E.V. Kumpjak, S.V. loginov, V. A. Sinebryuhov N. V. Tsou, V. V. Cervjakov, V. P. Yakovlev, and G. A. Mesyats, "Primary energy storages based on linear transformer stages", Laser and Particle Beams, vol. 21, no. 2, pp. 295–299, 2003.

[7] L. Zhou, Z. Li, Z. Wang et al., "Design of a 5-MA 100-ns linear-transformer-driver accelerator for wire array Z-pinch experiments," *Physical Review Accelerators and Beams*, vol. 19, no. 3, Article ID 30401, 2016.

[8] L. Chen, W. Zou, L. Zhou et al., "Development of a fusion-oriented pulsed power module," *Physical Review Accelerators and Beams*, vol. 22, no. 3, Article ID 30401, 2019.

[9] W. A. Stygar, M. E. Cuneo, D. I. Headley et al., "Architecture of petawatt-classz-pinch accelerators," *Physical Review Special Topics - Accelerators and Beams*, vol. 10, no. 3, Article ID 30401, 2007.

[10] W. A. Stygar, T. J. Awe, J. E. Bailey et al., "Conceptual designs of two petawatt-class pulsed-power accelerators for high-

energy-density-physics experiments," *Physical Review Special Topics—Accelerators and Beams*, vol. 18, no. 11, Article ID 110401, 2015.

[11] R. B. Spielman, D. Froula, G. Brent et al., "Conceptual design of a 15-TW pulsed-power accelerator for high-energy-density–physics experiments," *Matter and Radiation at Extremes*, vol. 2, no. 4, pp. 204–223, 2017.

[12] M. L. Kiefer and M. M. Widner, "Screamer-a single-line pulsed-power design tool," in *Proceedings of the Fifth IEEE Pulsed Power Conference*, Piscataway, NJ, USA, 1985.

[13] R. B. Spielman and Y. Gryazin, "Screamer v4.0-a powerful circuit analysis code," in *Proceedings of the IEEE Pulsed Power Conference (PPC)*, Piscataway, NJ, USA, 2015.

[14] D. D. Hinshelwood, *BERTHA: a versatile transmission line and circuit code*Naval Research Laboratory, Washington, D.C., USA, 1983.

[15] W. N. Weseloh, TLCODE—a transmission line code for pulsed power design, in *Proceedings of the 7th IEEE Pulsed Power Conference*, Piscataway, NJ, USA, 1989.

[16] S. Mirjalili and S. Z. M. Hashim, "A new hybrid PSOGSA algorithm for function optimization," in *Proceedings of the 2010 International Conference on Computer and Information Application*, Tianjin, China, 2010.

[17] W. A. Stygar, T. C. Wagoner, H. C. Ives et al., "Water-dielectric-breakdown relation for the design of large-area multi-megavolt pulsed-power systems," *Physical Review Accelerators and Beams*, vol. 9, no. 7, Article ID 70401, 2006.

[18] Z. Z. Gong, H. Wei, S. Y. Fan, F. J. Sun, and A. C. Qiu, "Inductance calculation of the central converging region of the high current Z-pinch driver," *Journal of Xi'an Jiaotong University*, vol. 56, no. 6, pp. 1–8, 2022.

[19] W. A. Stygar, G. A. Gerdin, and D. L. Fehl, "Analytic electrical-conductivity tensor of a nondegenerate lorentz plasma," *Physical Review*, vol. 66, no. 4, Article ID 46417, 2002.

[20] C. A. Jennings, J. P. Chittenden, M. E. Cuneo et al., "Circuit model for driving three-dimensional resistive MHD wire array Z-Pinch calculations," *IEEE Transactions on Plasma Science*, vol. 38, no. 4, pp. 529–539, 2010.

[21] J. Kennedy and R. C. Eberhart, "Particle swarm optimization," in *Proceedings of the IEEE International Conference on Neural Networks*, Perth, Australia, 1995.

[22] Y. Shi and R. C. Eberhart, "A modified particle swarm optimizer," in *Proceedings of the IEEE International Conference on Evolutionary Computation*, Anchorage, AK, USA, 1998.

[23] E. Rashedi, H. Nezamabadi-pour, and S. Saryazdi, "GSA: a gravitational search algorithm," *Information Sciences*, vol. 179, no. 13, pp. 2232–2248, 2009.

[24] W. A. Stygar, H. C. Ives, D. L. Fehl, M. E. Cuneo, M. G. Mazarakis, J. E. Bailey, G. R. Bennett, D. E. Bliss, G. A. Chandler, R. J. Leeper, M. K. Matzen, D. H. McDaniel, J. S. McGurn, J. L. McKenney, L. P. Mix, D. J. Muron, J. L. Porter, J. J. Ramirez, L. E. Ruggles, J. F. Seamen, W. W. Simpson, C. S. Speas, R. B. Spielman, K. W. Struve, J. A. Torres, R. A. Vesey, T. C. Wagoner, T. L. Gilliland, M. L. Horry, D. O. Jobe, S. E. Lazier, J. A. Mills, T. D. Mulville, J. H. Pyle, T. M. Romero, J. J. Seamen, and R. M. Smelser, "X-ray emission from z pinches at 10^7 A: current scaling, gap closure, and shot-to-shot fluctuations," *Physical Review*, vol. 69, pp. 266–289, 2004.

[25] W. A. Stygar, M. E. Cuneo, R. A. Vesey et al., "Theoreticalz-pinch scaling relations for thermonuclear-fusion experiments," *Physical Review E—Statistical Physics, Plasmas, Fluids, and Related Interdisciplinary Topics*, vol. 72, no. 2, Article ID 26404, 2005.